

Dynamics of Rotator Chain with Dissipative Boundary

Pu Ke¹ and Zhigang Zheng^{1,*}

¹*Department of Physics and the Beijing-Hong Kong-Singapore Joint Center for Nonlinear and Complex Systems(Beijing), Beijing Normal University, Beijing 100875, People's Republic of China*

We study the dynamical properties of rotator chain subjected to purely mechanical driving on the boundary by stability analysis and numerical simulation. Synchronized rotation, two-way synchronized rotation, and split synchronized rotation states are identified. In particular, we find the single-peaked variance distribution of angular momenta is the consequence of two-way synchronization. As a result, the operational definition of temperature used in previous studies on rotator chain should be revisited.

I. INTRODUCTION

The violation of Fourier's law in low dimensional lattice has drawn much attention in recent years due to its fundamental importance to non-equilibrium thermodynamics and statistical mechanics [1]. This phenomenological law, which relies on the local equilibrium hypothesis, is a macroscopic description of non-equilibrium process, and was verified to be accurate through various experimental settings. However, a rigorous derivation of Fourier's Law from microscopic statistical-mechanical argument is still missing, which motivated a large number of studies on energy conduction in various models. As an unexpected result drawn from these studies, Fourier's Law is violated for the divergence of heat conductivity with system size in many one dimensional the oscillator-based systems, unless substrate potential exists [2–4] or the interaction potential is asymmetrical [5].

The model of rotator chain was introduced as a counter example to oscillator-based models by the fact that it obeys Fourier's Law without any on-site potential when only thermal driving exists [6, 7]. Nevertheless, when both thermal and mechanical driving exist in this model, the variance profile of momenta, which is commonly used as the operational definition for temperature, is nonlinear, this fact seems directly contradicts Fourier's Law[8]. The origin of this nonlinearity need to be explained by specific dynamical properties of rotator chain. Although rotator chain model is a special case of the classical XY model, which drawn much attention in the fields of both extensive[9] and non-extensive[10] statistical mechanics, few studies have been focused on the dynamical properties of rotator chain, especially the variance profile of angular momenta.

The present paper focuses on the dynamical properties of the rotator chain that are subjected to purely mechanical driving. We proved the existence of synchronized rotation and identified two other dynamical states as parameters vary. The momenta variance profile was observed to be qualitatively similar to the case when both thermal and mechanical driving are presented. As further investigation, we also analyzed the momenta distribution,

detailed evolution information, and phase portrait of interface rotators. The results provided strong evidences that the nonlinear variance profile of angular momenta was of dynamical origin.

The paper is organized as follows. In Sec. II, a detailed description of rotator chain is presented and the existence of synchronized state is proved. Sec. III A discusses energy current, averaged momenta and momenta variance profiles. Sec. III B is devoted to an explanation to the nonlinearity of variance profiles by investigating rotation states of interface rotators. Finally, Sec. IV concludes the paper.

II. ROTATOR CHAIN

A. Description of the Model

A chain of N rotators is described by the angles $\phi = (\phi_1, \phi_2, \dots, \phi_N)$ and their conjugate angular momenta $L = (L_1, L_2, \dots, L_N)$, See Fig 1. The nearest-

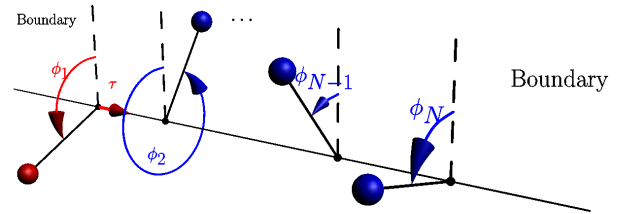


FIG. 1. (Color online) Illustration of a rotator chain.

neighbor interaction potential is periodical and takes the form

$$U(\phi_k, \phi_{k+1}) = \epsilon [1 - \cos(\phi_{k+1} - \phi_k)], \quad (1)$$

where ϵ is the coupling coefficient.

Moreover, the system is homogeneous, that is, the moments of inertia of all rotator are I . Therefore, the Hamil-

* zgzheng@bnu.edu.cn

tonian of the system is

$$\mathcal{H}(\phi, \mathbf{L}) = \sum_k \left\{ \frac{L_k^2}{2I} + \epsilon [1 - \cos(\phi_{k+1} - \phi_k)] \right\}. \quad (2)$$

Dissipation is introduced on the both end for consistency to the case when thermal driving exists (fluctuation-dissipation theorem). Introducing dimensionless time $s = \sqrt{\frac{\epsilon}{I}}t$ and letting $\omega_k = \frac{d\phi_k}{ds}$, the dimensionless equations of motion with open boundary reads

$$\begin{aligned} \frac{d\phi_k}{ds} &= \omega_k, \\ \frac{d\omega_k}{ds} &= \sin(\phi_{k+1} - \phi_k) - \sin(\phi_k - \phi_{k-1}), \quad k \neq 1, N \\ \frac{d\omega_1}{ds} &= \sin(\phi_2 - \phi_1) - \alpha\omega_1 + \tau, \\ \frac{d\omega_N}{ds} &= -\sin(\phi_N - \phi_{N-1}) - \alpha\omega_N, \end{aligned} \quad (3)$$

where α is the effective dissipation coefficient and τ is the effective torque.

B. Dynamical States of Rotator Chain

Depending on α and τ , the rotator chain has three kinds of dynamical states: *synchronized rotation state*, *split synchronized rotation state* and *two-way synchronized rotation state*.

In the synchronized rotation states, all rotators rotate at the same angular momentum. It can be proved that (see Sec. II B 2) for any α and $\tau < 2$, the synchronized rotation state is unique, and the phase difference of every adjacent rotator pair is $\pi - \arcsin(-\frac{\tau}{2})$ (c.f. (17)).

In the split synchronized rotation state, the driving rotator rotates as if the remaining rotators do not exists, while the remaining rotators rotate slowly in synchronization. This state could be attained when τ is sufficiently large.

In the two-way synchronized rotation state, the entire chain is divided into three region: fast rotation region, slow rotation region and interface region. In the fast and slow rotation region, the phase difference of the adjacent rotators oscillates around 0 and could not exceed 2π , while the rotators in the interface region exhibit complicated dynamical pattern – their rotations are affected by the rotators both in fast rotation region and slow rotation region.

As a preliminary investigation, it is instructive to consider the stability of the system analytically. In the next subsection, the uniqueness of stable fixed point of a rotator chain without dissipation is proved and a saddle-node bifurcation is identified; then the argument is extended to rotator chain with dissipative boundary to reveal the necessary condition $\tau > 2$ for the forming of nonlinear momenta variance profile.

1. Rotator Chain without Dissipative Boundary

Having introduced phase difference $\delta_k = \phi_{k+1} - \phi_k$ and its derivative $\Delta_k = \frac{d\delta_k}{ds}$, the equation of motion can be cast into ($\alpha = 0$)

$$\begin{aligned} \frac{d\delta_k}{ds} &= \Delta_k, \\ \frac{d\Delta_k}{ds} &= -2\sin\delta_k + \sin\delta_{k-1} + \sin\delta_{k+1}, \quad k \neq 1, N-1 \\ \frac{d\Delta_1}{ds} &= -2\sin\delta_1 + \sin\delta_2 - \tau, \\ \frac{d\Delta_{N-1}}{ds} &= -2\sin\delta_{N-1} + \sin\delta_{N-2}. \end{aligned} \quad (4)$$

The general formula of $\frac{d\Delta_k}{ds} = 0$ is $\sin\delta_k = k\sin\delta_1$, then the only possible solution is $\sin\delta_k = 0$ (i.e. $\delta_k = n_k\pi$). The Jacobian matrix of (4) is

$$\mathbf{J} = \begin{pmatrix} \mathbf{0} & \mathbf{I}_{N-1} \\ \mathbf{C} & \mathbf{0} \end{pmatrix}, \quad (5)$$

where \mathbf{I}_{N-1} is $N-1$ th order unit matrix, and \mathbf{C} is

$$\begin{pmatrix} -2\chi_1 & \chi_2 & 0 & 0 & \cdots & 0 \\ \chi_1 & -2\chi_2 & \chi_3 & 0 & \cdots & 0 \\ 0 & \chi_2 & -2\chi_3 & \chi_4 & \cdots & 0 \\ \vdots & \vdots & \vdots & \ddots & \ddots & \vdots \\ 0 & 0 & 0 & 0 & \chi_{N-2} & -2\chi_{N-1} \end{pmatrix}, \quad (6)$$

where $\chi_k = \pm 1$. The eigenequation of Jacobian Matrix is

$$\begin{aligned} \det \begin{pmatrix} -\lambda\mathbf{I}_{N-1} & \mathbf{I}_{N-1} \\ \mathbf{C} & -\lambda\mathbf{I}_{N-1} \end{pmatrix} \\ = \det(-\lambda\mathbf{I}_{N-1}) \times \det(-\lambda\mathbf{I}_{N-1} + \mathbf{C}\frac{1}{\lambda}) \\ = (-1)^{N-1} \det(\mathbf{C} - \lambda^2\mathbf{I}_{N-1}) = 0. \end{aligned} \quad (7)$$

Which implies the eigenvalues of \mathbf{J} are square roots of the eigenvalues of \mathbf{C} .

If all $\chi_k = 1$ ($\delta_k = 2n_k\pi$), then the eigenvalues of \mathbf{C} are $\lambda^2 = -2(1 + \cos\frac{k\pi}{N}) < 0$ ($k = 1, \dots, N-1$) [11]. Since λ s are purely imaginary, $\delta_k = 2n_k\pi$ corresponds to a center in phase space.

Suppose that at least one $\chi_r = -1$ ($r < N-1, \delta_r = (2n+1)\pi$), then from Gershgorin's Theorem [12], for eigenvalue λ_r^2 of \mathbf{C} , $|\lambda_r^2 - 2| \leq 2$. Because matrix \mathbf{C} is nonsingular (all columns are linear independent), then $\text{Re}\lambda_r > 0$, which renders the fixed point unstable. The argument still holds when more than one $\chi = -1$, since the sum of all off-diagonal elements on arbitrary row is smaller than 2.

As proved above, the only stable fixed point of equation (4) is $\delta_k = 2n_k\pi$, which is a center. The corresponding motion is collective rotation with phase difference and its derivative of each pair of rotator oscillate around $(2n_k\pi, 0)$ (Libration).

If driving torque is added at the boundary, the general formula of $\frac{d\Delta_k}{ds} = 0$ becomes $\sin \delta_k = k \sin \delta_1 + (k-1)\tau$. Substituting it into $\frac{d\Delta_{N-1}}{ds} = 0$ gives the necessary condition for the existence of fixed points $\sin \delta_1 = \frac{1-N}{N}\tau$. Assume the chain is sufficiently long, then $\lim_{N \rightarrow \infty} \sin \delta_1 = -\tau$, and $\tau = 1$ is a saddle-node bifurcation point.

2. Rotator Chain with Dissipative Boundary

The role of the boundary rotators is of crucial importance in the formation of nonlinear variance profile. Consider a system consists of only two boundary rotators

$$\begin{aligned} \frac{d\delta}{ds} &= \Delta, \\ \frac{d\Delta}{ds} &= -2\sin \delta - \alpha\Delta - \tau. \end{aligned} \quad (8)$$

Introducing new time scale $\xi = \sqrt{2}s$, then the equation transform to

$$\frac{d^2\delta}{d\xi^2} = -\sin \delta - \eta \frac{d\delta}{d\xi} - \beta, \quad (9)$$

where $\eta = \frac{\sqrt{2}}{2}\alpha$ and $\beta = \frac{\tau}{2}$. Despite the minus sign, equation (9) is the governing equation for the Josephson junction, and received extensive study[13]. Depending on the effective dissipation coefficient η and the effective torque β , we can observe three kinds of bifurcation: homoclinic, infinite-period and saddle-node bifurcation. The saddle-node and the homoclinic bifurcation matters here, if $\beta > 1$ then there is no fixed point in the phase plane, all trajectories are attracted to a unique, stable limit cycle(c.f. Fig. 2(c))[14]; limit cycle and stable spiral point could also coexist(bistable state c.f. 2(b)) if $\beta < 1$ and η is sufficiently small, but there is no general analytical formula for the homoclinic bifurcation curve. Limit cycle corresponds to unsynchronized rotation; while when $\beta < 1$, it is possible that two rotator phase-locked(c.f. Fig. 2(a)). The existence of a saddle-node bifurcation point in rotator chain with boundary rotators will be proved in the next paragraph and further corroborated by numerical simulation in Sec. III A.

The phase difference equation of (3) is

$$\begin{aligned} \frac{d\delta_k}{ds} &= \Delta_k, \\ \frac{d\Delta_k}{ds} &= -2\sin \delta_k + \sin \delta_{k-1} + \sin \delta_{k+1}, \quad k \neq 1, N-1 \\ \frac{d\Delta_1}{ds} &= -2\sin \delta_1 + \sin \delta_2 + \alpha\omega_1 - \tau, \\ \frac{d\Delta_{N-1}}{ds} &= -2\sin \delta_{N-1} + \sin \delta_{N-2} - \alpha\omega_N, \end{aligned} \quad (10)$$

and the phase difference equation for two boundary ro-

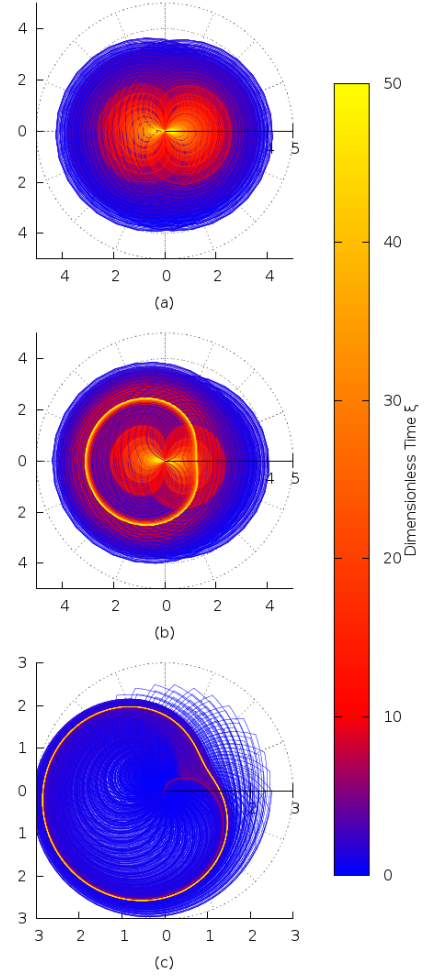


FIG. 2. (Color online) Phase portrait of (9) in polar coordinate, azimuth represents phase difference and radius represents time derivative of phase difference. (a) $\eta = 0.1, \beta = 0.027$, only fixed points existed (b) $\eta = 0.1, \beta = 0.037$, bistable state: fixed points and limit cycle coexisted (c) $\eta = 0.1, \beta = 1.1$, only limit cycle existed.

tators ($\delta_{1,N} = \phi_N - \phi_1$) is

$$\begin{aligned} \frac{d\delta_{1,N}}{ds} &= \Delta_{1,N}, \\ \frac{d\Delta_{1,N}}{ds} &= \frac{d\omega_N}{ds} - \frac{d\omega_1}{ds}, \\ &= -\sin \delta_{N-1} + \sin \delta_1 - \alpha\Delta_{1,N} - \tau. \end{aligned} \quad (11)$$

The condition $\frac{d\Delta_k}{ds} = 0$ can be rewritten in the form of forward and backward recurrent equation

$$\begin{aligned} \sin \delta_k &= 2\sin \delta_{k-1} - \sin \delta_{k-2} & k \geq 3 \\ \sin \delta_{N-k} &= 2\sin \delta_{N-k+1} - \sin \delta_{N-k+2} & k \geq 3 \end{aligned} \quad (12)$$

Solving $\frac{d\Delta_{1,N}}{ds} = 0$ for $\sin \delta_1$ and substitute the result into $\frac{d\Delta_{N-2}}{ds} = 0$ gives the initial value for backward recurrence

equation

$$\begin{aligned}\sin \delta_{N-1} &= -\sin \delta_1 - \tau, \\ \sin \delta_{N-2} &= -2\sin \delta_1 + \alpha\omega_N - 2\tau.\end{aligned}\quad (13)$$

The initial value of forward recurrence equation is straightforward from $\frac{d\Delta_1}{ds} = 0$

$$\begin{aligned}\sin \delta_1 &= \sin \delta_1, \\ \sin \delta_2 &= 2\sin \delta_1 - \alpha\omega_1 + \tau.\end{aligned}\quad (14)$$

Then the general formulae for forward and backward recurrence equation can be obtained

$$\begin{aligned}\sin \delta_k &= k\sin \delta_1 + (k-1)(\tau - \alpha\omega_1), \\ \sin \delta_{N-k} &= -k\sin \delta_1 - k\tau + \alpha(k-1)\omega_N,\end{aligned}\quad (15)$$

the necessary condition for fixed points then follows ($\Delta_{1,N} = \omega_N - \omega_1 = 0$)

$$\sin \delta_k + \sin \delta_{N-k} = -\tau. \quad (16)$$

The only solution that satisfies (16) and $\frac{d\delta_k}{ds} = 0$ simultaneously is

$$\sin \delta_k = -\frac{\tau}{2}. \quad (17)$$

It is evident that $\tau = 2$ is a saddle-node bifurcation point, if $\tau > 2$, then there could not be any fixed point, and the entire system could not be synchronized. Numerical simulation confirmed that $\tau > 2$ is a necessary condition for nonlinear variance profile to form.

The argument of last subsection still holds, the only differences are $\chi = \pm\sqrt{1 - \frac{\tau^2}{4}}$ and elements in Jacobian regarding $\Delta_{1,N}$ that render the stable fixed point a spiral.

The above result shows under the condition $\tau < 2$ the rotator chain with dissipative boundary could have the possibility of synchronized collective rotation.

When $\tau > 2$, it can be proved that there exist trajectories of (10) that are confined in the energy shell E_r . E_r is determined by $\frac{dE}{ds} = \omega_1(\tau - \omega_1) - \omega_N^2 < 0$, if $\omega_1 > \tau$, then the inequality holds under any condition, then $E_r = N(\frac{\tau^2}{2} + 2)$. The determination of the types of trajectories calls for further studies on Poincaré-Bendixson type theorem in N-dimensional space.

With synchronized rotation, nonlinear profile of angular momenta is impossible, since the momentum variance of each rotator is identically 0, which indicate $\tau > 2$ is a necessary condition for nonlinear profile to form.

III. NUMERICAL SIMULATION

The system of equations (3) had been integrated numerically by Velocity-Verlet and Gear's Predictor-Corrector algorithm[15] for a chain of 1024 rotators with time step size $\Delta s = 0.01$, while there is some time-step bias in the value of the fluxes, both methods produced

the same qualitative results with respect to the choice of the time step.

The variance of momentum is defined as

$$\begin{aligned}\text{var}\{\omega_k\} &= \langle (\omega_k - \langle \omega_k \rangle)^2 \rangle = \langle \omega_k^2 \rangle - \langle \omega_k \rangle^2 \\ &= \lim_{s \rightarrow \infty} \frac{1}{s} \int_0^s \omega_k^2(\zeta) d\zeta - \left[\lim_{s \rightarrow \infty} \frac{1}{s} \int_0^s \omega_k(\zeta) d\zeta \right]^2.\end{aligned}\quad (18)$$

and the local energy flux is computed by[16]

$$j_k = \lim_{s \rightarrow \infty} \frac{1}{2s} \int_0^s [\omega_k(\zeta) + \omega_{k+1}(\zeta)] F[\phi_{k+1}(\zeta) - \phi_k(\zeta)] d\zeta. \quad (19)$$

Define the norm of a solution vector $\mathbf{V} = (\phi)$ to be

$$|\mathbf{V}| = \sqrt{\sum_k (\phi_k^2 + \omega_k^2)}. \quad (20)$$

Note that the norm has the property $|\mathbf{V}| = 0$ if and only if $\mathbf{V} = \mathbf{0}$.

The fixed boundary conditions were also checked numerically, this is equivalent to adding extra torques $-\sin \phi_k$ ($k = 1, N$) on each end. In particular, a rotator chain with both kinds of boundary condition had single-peaked variance profile of momenta in certain parameter region.

All observables were analyzed for the time scales of $10^8 - 10^{10}$, when the system relaxed to steady state.

A. An Overview of the Dynamical States

The energy flux is plotted for revealing the overall dynamical states of the rotator chain.

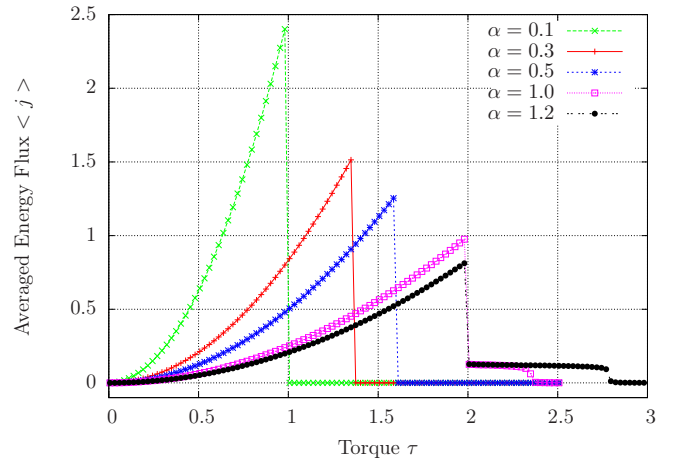


FIG. 3. (Color online) Averaged energy flux of rotator chain.

As the driving torque increased, the torque-flux curve exhibited three qualitatively different segments for all $\alpha > 1$. When $\tau < 2$, the local energy flux increased monotonically with driving torque as $\langle j \rangle = \frac{\tau^2}{4\alpha}$, while

identically plunged when $\tau > 2$, and virtually vanished if mechanical torque is larger than $2.636\alpha - 0.437$. For the cases $\alpha < 1$, the local energy flux dropped when $\tau < 2$. We have proved rotator chain without dissipative boundary has a saddle-node bifurcation point $\tau = 1$ (c.f. IIB1). As the effective dissipation coefficient α decreased, $\frac{d\Delta_1}{ds}$ in transient state could be too large for the synchronized rotation (c.f. FIG. 2(b)), which rendered the rotator chain in *split synchronized rotation state*.

The monotonic relation between the averaged energy flux and the driving torque is straightforward from the result derived in IIB2. Assume that the system had relaxed to the spiral, then $\Delta_{1,N} = \omega_N - \omega_1 = 0$ and $\sin \delta_k = \frac{\tau}{2}$. For the total energy E of the system $\frac{dE}{ds} = 0$, the work done by driving torque must be balanced by the dissipation at both end $\tau\omega = 2\alpha\omega^2$, combined with (10) we conclude that at spiral all rotators have same angular momenta $\omega = \frac{\tau}{2\alpha}$. Substituting this result and (17) into (19) leads to the relation $\langle j \rangle = \frac{\tau^2}{4\alpha}$. The proof provides strong evidence that the monotonically increasing segment represent the synchronized rotation state of rotator chain.

The averaged momenta and the variance of momenta are plotted for analyzing each segment of the curve for $\alpha = 1.0$ in FIG. 3. As expected, the curves that are corresponded to each segments are essentially different, see FIG. 4. The three segments in the cases $\alpha > 1$ correspond to *synchronized rotation*, *two-way synchronized rotation* and *split synchronized rotation* respectively.

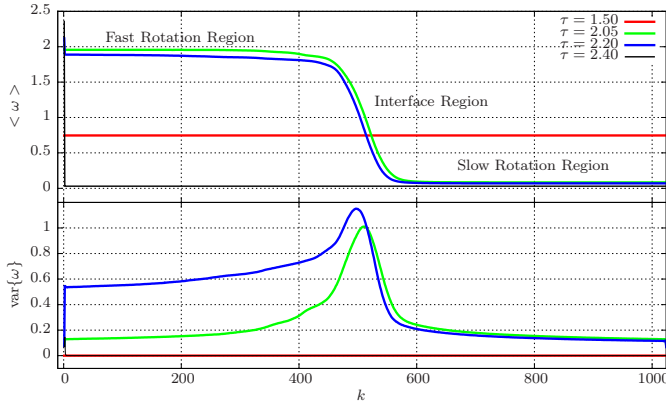


FIG. 4. (Color online) Averaged momenta and variance of momenta for chains of $\alpha = 1.0$.

The entire chain was synchronized when $\tau = 1.5, \alpha = 1.0$, as predicted in IIB2 (Noting that the momentum of every rotator are exactly $\frac{\tau}{2\alpha}$). As the effective torque further increased, an interface area where averaged momenta exhibited significant drop emerged, and the entire chain was divided into three regions: 1. *Fast rotation region* 2. *Interface region* and 3. *Slow rotation region*, the onset of interface region shifted left slightly as driving torque increased in this state. If the driving torque is sufficiently large, the driving rotator will rotated as if the remaining rotators on the chain do not exist (note

that $\omega \approx \tau$), this fact corresponded to the transform from librations to rotations in the single pendulum.

The momenta variance remained 0 when $\tau < 2$ (i.e. the rotator chain was synchronized), which confirm the results derived in IIB. When τ was sufficiently large, only several rotators near the driving rotator had nonzero momenta variance. This fact brought the name *split synchronized state*, despite the first several rotators, the remaining rotators had the same averaged momenta as well as zero variance of momenta, the entire chain thus consists of only one fast moving rotator while the others relaxed to slow synchronized rotation.

The phase trajectory of split synchronized rotation state is a closed orbit while the two-way synchronized state is not. This can be shown by calculating the reduced norm $\frac{|\mathbf{V}(s) - \mathbf{V}(s_0)|}{\max\{|\mathbf{V}(s) - \mathbf{V}(s_0)|\}}$, as shown in FIG. 5. The first two figures represent split synchronized states, and the last one represents two-way synchronized state.

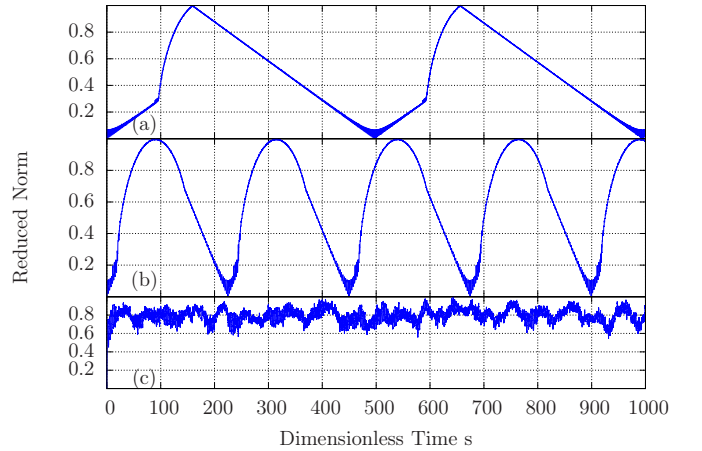


FIG. 5. (Color online) $\frac{|\mathbf{V}(s) - \mathbf{V}(s_0)|}{\max\{|\mathbf{V}(s) - \mathbf{V}(s_0)|\}}$ for (a) $\tau = 1.7, \alpha = 0.5$, (b) $\tau = 2.5, \alpha = 1.0$ and (c) $\tau = 2.2, \alpha = 2.2$.

It is interesting to note that the single-peaked distribution of variance existed when the rotator chain was in the *two-way synchronized* state and the peaks located in the interface region. In previous study, this form of variance profile was thought as a consequence of interaction between thermal and mechanical driving [8]. However in our model, thermal bath was clearly absent, hence the cause of single-peaked variance profile calls for further investigation by exploring the dynamical properties of interface rotators.

B. Rotation States of Interface Rotators

In order to trace the origin of large variance on the chain it is reasonable to analyze the momentum distribution of typical rotators. As shown in FIG. 6, the typical rotators in fast rotation region (e.g 1 and 400) had angular momenta distributions that was symmetrical about

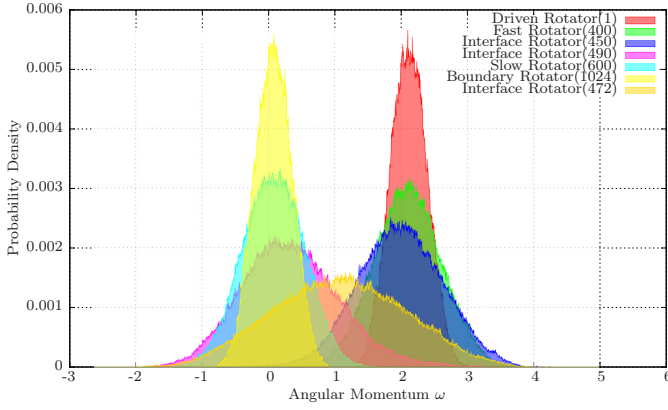


FIG. 6. (Color online) Distribution of angular momenta for $\tau = 2.2, \alpha = 1.0$.

the maximum value of angular momentum whereas those in slow rotation region (e.g 600 and 1024) had angular momenta distributions around zero. It is interesting to note that the rotators in the interface region(450, 472 and 490) had a momenta distribution extended from slow rotation region to fast rotation region, which provided the evidence that the rotators locate in the interface region constantly switched between the slow rotation state and fast rotation state, which result in large variance.

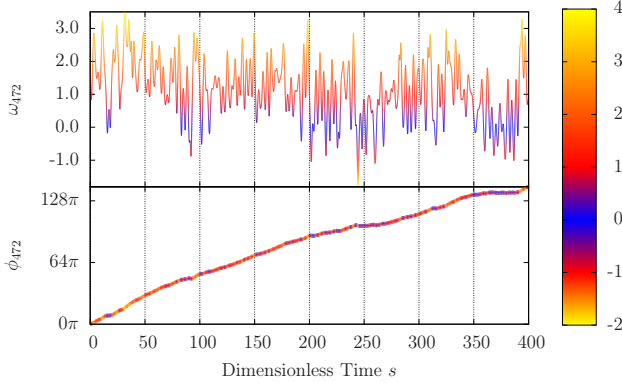


FIG. 7. (Color online) Evolution of angle and angular momentum (rotator 472) for $\alpha = 1.0, \tau = 2.2$.

For a clearer view, the evolution of angular momentum for an interface rotator is plotted in FIG. 7. The oscillation between fast rotation and slow rotation can then be easily spotted.

It has been proved in IIB2 that the boundary rotators can not be synchronized when $\tau > 2$, as illustrated in FIG. 8(a). Nevertheless, the adjacent interior rotators had different synchronization states. For the adjacent rotator pairs in either fast rotation region and slow rotation region, the phase difference and its derivative oscillate around $(0, 0)$, which corresponded to librations in single

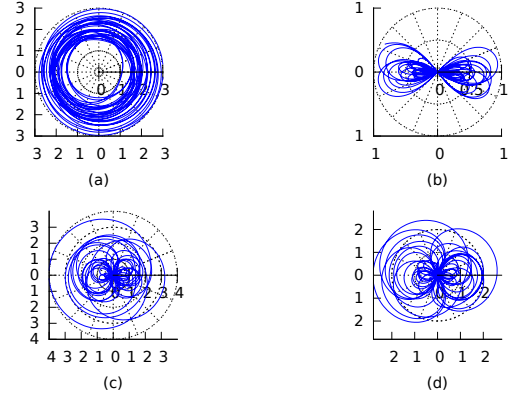


FIG. 8. (Color online) Phase portrait for phase difference of (a) two boundary rotators (b) two adjacent rotators in fast rotation region (c) interface rotator 472 and rotator 471 (d) interface rotator 472 and 473 ($\alpha = 1.0, \tau = 2.2$).

pendulum(See FIG. 8(b)). The case of rotator pairs in the interface is more complicated, the phase difference between both left and right rotators constantly shifted between librations to rotations and vice versa(See FIG. 8(c) and (d)), which accounted for the oscillation between fast rotation and slow rotation in the interface rotators. Since rotators in both fast rotation region and slow rotation region are separately synchronized, and interface rotators temporarily synchronize to both side, hence the name *two-way synchronization* is designated.

IV. CONCLUSION

The investigations presented above demonstrates that the dynamics of rotator chain with mechanical driving and dissipative boundary depends on the driving torque τ and the effective dissipation coefficient α .

Three dynamical states are identified for $\alpha > 1$. *Synchronized rotation* is proved to exist when $\tau < 2$. *split synchronized rotation* state emerges when τ is sufficiently large so that no other rotators on the chain could be synchronize with the driving rotator. *Two-way synchronized rotation* results from interior rotators' partial synchronization to each boundary.

The existence of the single-peaked variance profile of momenta is confirmed in the absence of heat bath, and the large variance in the interface region is the consequence of two-way synchronization state. Temperature is commonly defined as variance of momenta in the research of heat conduction problem in low dimensional system. But as our study shows, the variance profile of momenta could be the consequence of dynamical properties exclusively, and has no implication with heat. Moreover, a rotator chain with mechanical driving has three kinds of dynamical states rather than mere oscillation in the case of oscillator-based systems. Thermal driving could induce transitions between these states, thus whether the

operational definition of temperature used in oscillator-

based system is appropriate in rotator chain still calls for further investigation.

-
- [1] A. Dhar, [Advances in Physics](#) **57**, 457 (2008).
 - [2] S. Lepri, R. Livi, and A. Politi, [Phys. Rev. Lett.](#) **78**, 1896 (1997).
 - [3] G. Casati, J. Ford, F. Vivaldi, and W. M. Visscher, [Phys. Rev. Lett.](#) **52**, 1861 (1984).
 - [4] A. V. Savin and O. V. Gendelman, [Phys. Rev. E](#) **67**, 041205 (2003).
 - [5] Y. Zhong, Y. Zhang, J. Wang, and H. Zhao, [Phys. Rev. E](#) **85**, 060102 (2012).
 - [6] C. Giardinà, R. Livi, A. Politi, and M. Vassalli, [Phys. Rev. Lett.](#) **84**, 2144 (2000).
 - [7] O. V. Gendelman and A. V. Savin, [Phys. Rev. Lett.](#) **84**, 2381 (2000).
 - [8] A. Iacobucci, F. Legoll, S. Olla, and G. Stoltz, [Phys. Rev. E](#) **84**, 061108 (2011).
 - [9] D. R. Nelson and D. S. Fisher, [Phys. Rev. B](#) **16**, 4945 (1977).
 - [10] C. Anteneodo and C. Tsallis, [Phys. Rev. Lett.](#) **80**, 5313 (1998).
 - [11] D. Kulkarni, D. Schmidt, and S.-K. Tsui, [Linear Algebra and its Applications](#) **297**, 63 (1999).
 - [12] R. A. Horn and C. R. Johnson, *Matrix Analysis*, 2nd ed. (Cambridge University Press, 2012).
 - [13] M. Levi, F. Hoppensteadt, and W. Miranker, *Q. Appl. Math.*; (United States) **37** (1978).
 - [14] S. H. Strogatz, *Nonlinear Dynamics And Chaos: With Applications To Physics, Biology, Chemistry, And Engineering (Studies in Nonlinearity)*, 1st ed. (Westview Press, 2001).
 - [15] J. M. Haile, *Molecular Dynamics Simulation: Elementary Methods (Wiley Professional)*, 1st ed. (Wiley-Interscience, 1997).
 - [16] S. Lepri, R. Livi, and A. Politi, [Physics Reports](#) **377**, 1 (2003).